Nuclear Instruments and Methods in Physics Research A249 (1986) 277–295
North-Holland, Amsterdam

CALIBRATION AND MONITORING OF THE ARGUS SHOWER COUNTERS

A. DRESCHER, U. MATTHIESEN, H. SCHECK, B. SPAAN, J. SPENGLER and D. WEGENER
Institut für Physik, Universität Dortmund, FRG

R. HELLER *, K.R SCHUBERT, J. STIEWE and S. WESELER
Institut für Hochenergiephysik, Universität Heidelberg, FRG

Received 17 February 1986

The 1760 shower counter modules of the detector ARGUS at DORIS II are monitored by a laser as the central light source. A lead glass counter, which also detects cosmic muons, and a photodiode serve as reference systems. The paper describes the technical layout, performance and stability of the monitoring system. Algorithms and corrections applied in the calibration procedure are discussed in detail. The monitoring system serves also to control the time-of-flight counter performance and to calibrate their TDCs.

1. Introduction

The following paper describes calibration and monitoring procedures for the shower counter system of the detector ARGUS, operating since 1982 at the electron–positron storage ring DORIS II at DESY.

ARGUS is a normal conducting magnetic detector with cylindrical symmetry around the beam axis (fig. 1). A particle originating at the interaction vertex travels through the vertex drift chamber, the main drift chamber [1a], the time-of-flight system [1b], the shower counter system [1c], and finally the muon detection proportional tube system [1d]. The drift chamber is the central part of the detector; it measures charged particles' momenta and their specific energy loss by ionization. The chamber is surrounded by 64 barrel and 2×48 end cap time-of-flight scintillation counters. The barrel counters are viewed by two, the end cap counters by one phototube each. The time-of-flight counter system is followed by the shower counter calorimeter which again is divided into a barrel and two end cap parts. The barrel contains 1280 counter modules, the end caps contain 240 modules each.

A single shower counter module is a lead–scintillator sandwich coupled to its light guide through a wavelength shifter (fig. 2). A 1 mm lead plate is followed by a 5 mm scintillator layer. The total depth is 12.5 radiation lengths. To meet the geometrical conditions of the barrel, one counter module has a constant rectangular cross section ("plane parallel"), while its neighbour in azimuth has a "wedge" shape. The shower calorimeter is located inside the magnet coil.

* Now at DESY, Hamburg, FRG.

The paper is organized as follows: first, we give a detailed description of the monitoring system, its principle, technical and electronic layout, the reference systems used, and its stability with time. Next, we describe the calibration procedure for the shower counters, the corrections to be applied, and the algorithms to determine photon direction parameters. We discuss the time stability of the calibration achieved.

2. The monitoring system and its performance

2.1. General scheme of the monitoring system

A shower counter absorbs the energy E_γ of an incoming photon and emits an electronic signal whose height is proportional to E_γ. The factor of proportionality must be determined in a calibration procedure. Only ideally this factor is a constant; as a matter of fact it will depend on time, taking into account changes in performance of the readout system, mainly changing of phototube amplification. Therefore, measuring photon energies requires a permanent knowledge of the calibration factor. The procedure which provides this knowledge is called monitoring.

In the ARGUS shower counters, the photon energy is transformed into scintillation light which is detected by phototubes. A monitoring scheme must therefore supply an independent, well known and stable source of light which has to serve all counter phototubes plus reference tubes at a time. A possible realisation of such a central source is a high intensity laser.

Unfortunately, such a central light source is not absolutely stable. While short term fluctuations cancel

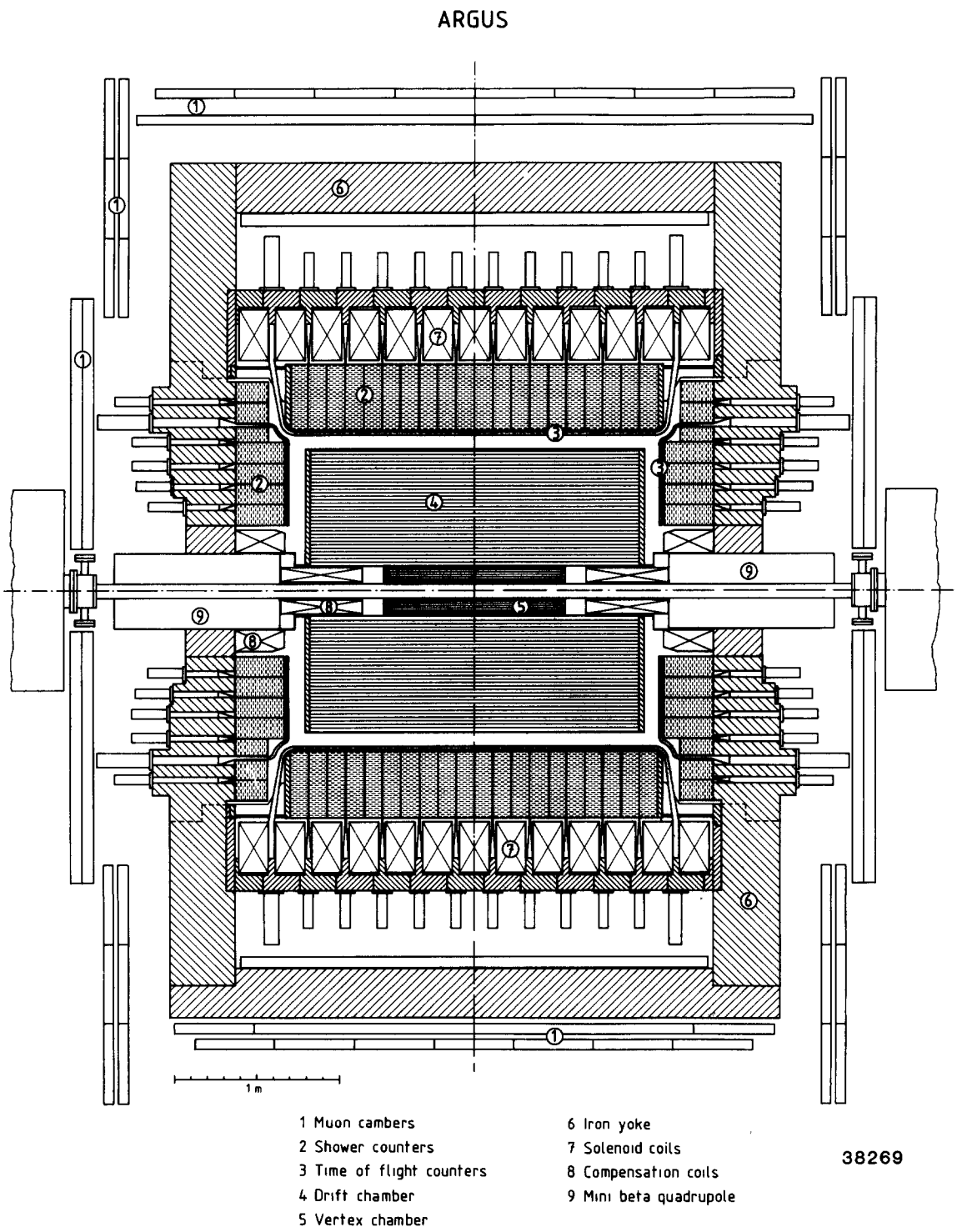

Fig. 1. Sketch of the detector ARGUS at DORIS II.

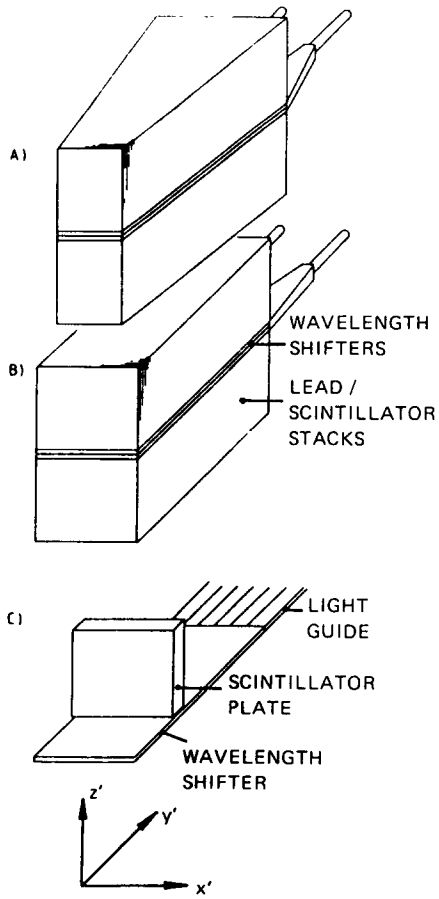

Fig. 2. Sketch of the ARGUS shower counter modules: a) wedge, b) plane parallel model. c) coordinate system used for shower counter studies.

according to the procedure described below, long time changes have to be controlled, too. This can be done using a reference phototube and a highly stable reference light source of low intensity as it is supplied by cosmic muons producing Cherenkov light in a lead glass block [2]. A block diagram of the monitoring system described below is shown in fig. 3.

The information necessary to readjust the calibration factors is then contained in the ratio between the shower counter pulse height at $\tau = 0$, i.e. at the beginning of the experiment, and that at the actual time τ. The change in performance is controlled by the monitor. Thus, the actual pulse height P_i of a shower counter is converted to the correct energy E_i with the help of calibration constants CAL_i and monitor signals in the following way:

$$E_i = P_i(\tau)\mathrm{CAL}_i \frac{\mathrm{MON}_i(0)}{\mathrm{MON}_i(\tau)}. \qquad (1)$$

This relation holds for each individual counter tube

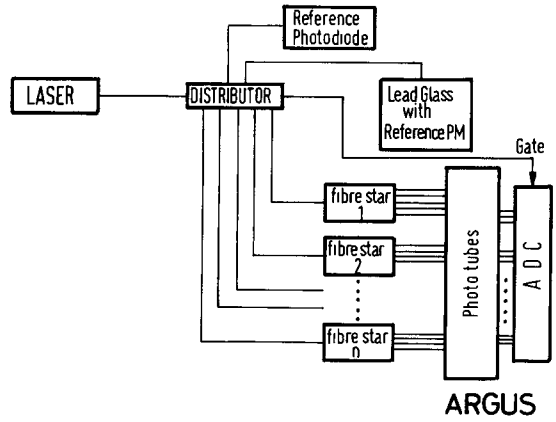

Fig. 3. Block diagram of the monitoring system.

i. The expression $\mathrm{MON}_i(\tau)$ is composed of counter and reference signal as follows:

$$\mathrm{MON}_i(\tau) = \left\langle \frac{P^i_{\mathrm{TUBE}}(\tau)}{P_{\mathrm{REF}}(\tau)} \right\rangle \langle P_{\mathrm{RefCos}}(\tau) \rangle \qquad (2)$$

Here P^i_{TUBE} denotes the counter pulse height and P_{REF} the reference PM pulse height, both produced by the laser. P_{RefCos} denotes the pulse height from cosmic muons, as seen by the reference phototube. The brackets denote averages over approximately 200 pulses.

2.2. Technical layout of the monitoring system

For the ARGUS shower and time-of-flight counters, a laser was chosen as the central monitoring light source [3]. The laser light is fed, with the help of a distribution system, into each single shower and time-of-flight counter module, to a photodiode, and, via a lead glass block, to a reference phototube. The lead glass Cherenkov counter serves also as the cosmic reference system. The layout of the monitoring system is shown in fig. 4.

The central light source is a nitrogen laser * which emits ultraviolet light at a wavelength of 337.1 nm. The laser consists of a spark gap with a low nitrogen flow; it is fired by a short 15 kV pulse which is supplied to the spark electrodes when a trigger pulse arrives. The trigger pulse fires a second trigger spark gap which mediates the discharge of the laser gap. The laser gap emits a high intensity short light pulse with a rise time of less than 100 ps. This so called super-radiation is less monochromatic than light from a genuine laser and does not contain its degree of coherence. The properties of the laser are summarized in table 1

* LN 100, PRA Inc. Canada, modified by the electronic workshop of the Heidelberg institute.

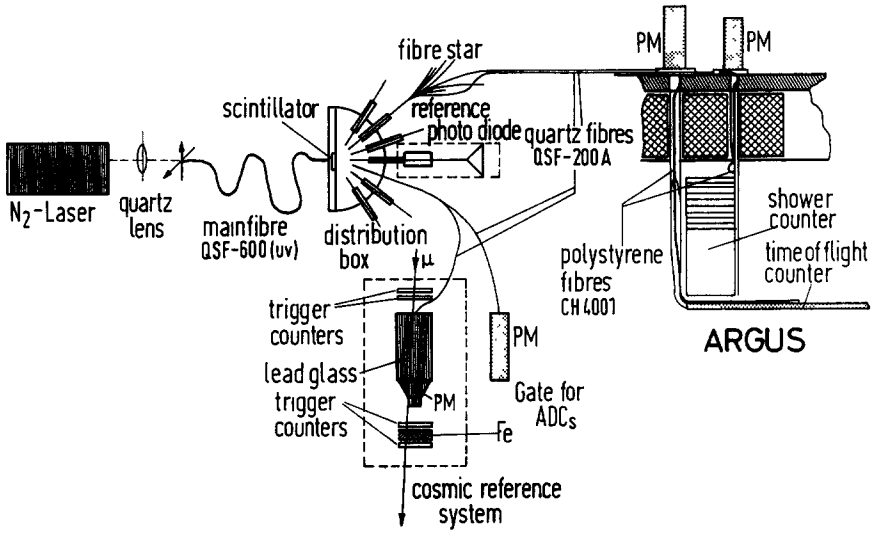

Fig. 4. Technical layout of the monitoring system.

Table 1
Properties of the nitrogen laser LN 100

Wave length	337.1 nm
Pulse energy	60 μJ at 1 atm
Pulse width	100–300 ps
Repetition rate	0–100 Hz, single shot or external trigger
Beam divergency	3.7 mrad at 1 atm

The laser is positioned in the control room, some 10 meters away from the detector, and its light has to be transported to the counter modules by an optical fibre system.

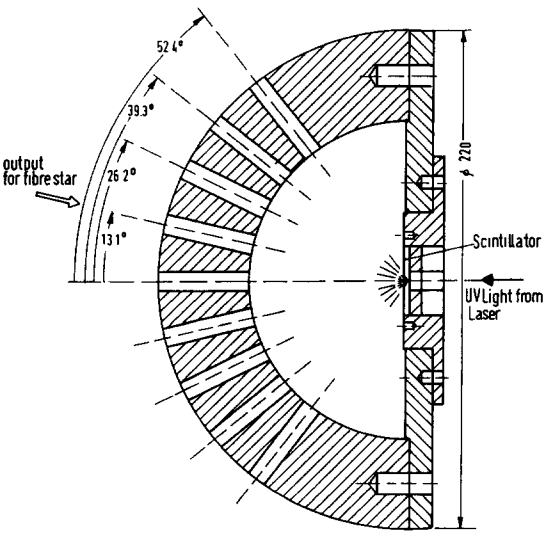

Fig. 5. Section through the light distribution box.

The ultraviolet light is focused by a quartz lense (focal length = 10 cm) to the entrance surface of a quartz fibre ** with a diameter of 0.6 mm and a length of 30 m. This fibre is especially transparent for UV light; its effective attenuation length for the wavelength considered was found to be 45 m. The other end of the quartz fibre is fed into the distribution box (fig. 5) which is situated inside the detector yoke, close to the counter modules. It is a brass hemisphere with an input opening for the quartz fibre and 55 output openings for further light distribution: 48 for the fibre stars, two for the reference counters, one for the gate generating phototube, and four spares. The incoming laser light is absorbed by a small piece of scintillation material (NE 110) and re-emitted at larger wavelengths. This secondary light is viewed by the distribution stars, each containing 45 resp. 39 single fibres *** which point radially to the centre of the hemisphere where the scintillator is fixed. In total, more than 2000 fibres are served in this way. The two ends of a distribution connector are shown in fig. 6. The fibres are made of quartz; their diameter is 0.2 mm, their lengths are adjusted individually. The light distributors have been manufactured by Laaber Faseroptik GmbH, Rüsselsheim, Germany. They guide the light to the phototube housings which are located outside the coil (barrel region) resp. outside the yoke (end cap region). Here they are coupled to polystyrene fibres † of 1 mm thickness with the help of a brass connector. The additional connection facilitates handling the counters; furthermore, the final part of the light transport system is

** QSF-600 (UV), Quartz & Silice, Paris, France.
*** QSF-200A, Quartz & Silice, Paris, France.
† CH 4001, Distributor: ELPAC, München, Germany.

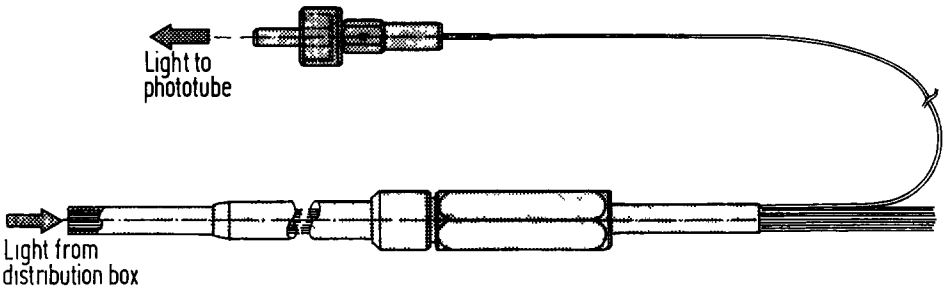

Fig. 6. Light distributor with connectors.

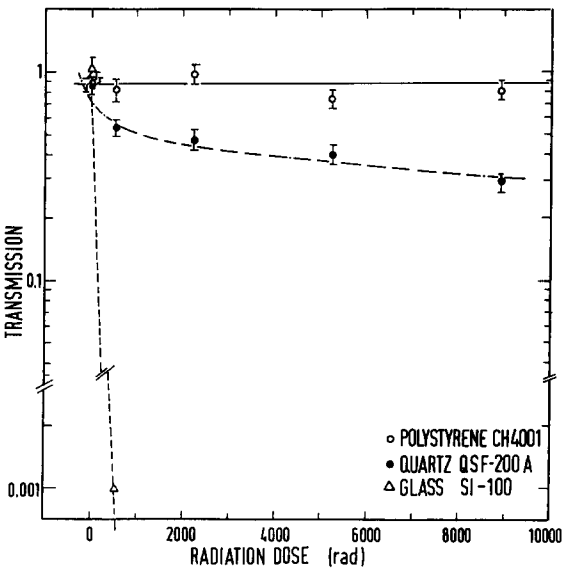

Fig. 7. Relative transmission versus radiation dose for glass, quartz, and polystyrene fibres.

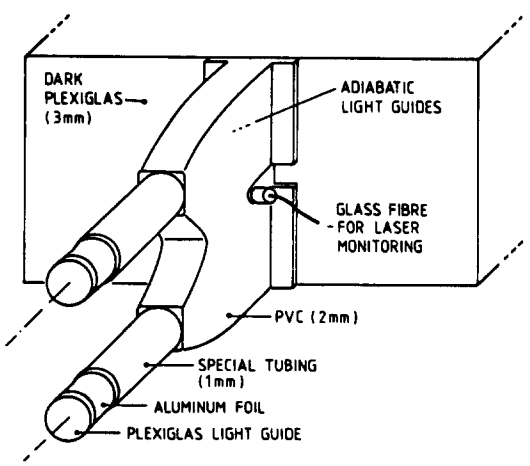

Fig. 8. Sketch of the light feed-in system for a shower counter module.

Table 2
Properties of the light transport fibres used

Fibre type	QSF-200 A	QSF-600 (UV)	CH 4001
Fibre diameter	200 μ	600 μ	1000 μ
Num. aperture	0.3 rad	0.3 rad	0.5rad
Absorption length	45 ± 3 m at $\lambda = 436$ nm	45 ± 3 m at $\lambda = 337.1$ nm	6.3 ± 0.5 m at $\lambda = 436$ nm

exposed to synchrotron radiation which might damage the fibres. Test measurements performed at the Heidelberg betatron have shown that polystyrene has a resistence against radiation much higher than quartz and other materials (see fig. 7).

The final coupling between polystyrene fibres and counters is handled in different ways for shower and time-of-flight counters. In case of the shower counters, the fibre ends in a small plexiglass cylinder of 8 mm diameter. The plexiglass cylinder in turn is glued [††] directly to the wavelength shifter material of the shower counter. Fig. 8 shows the arrangement for feeding the light into the shower counter modules. In case of the time-of-flight barrel counters, the fibres end in small plexiglass prisms wich are glued [†††] to the counter surface centrally. The prisms are covered with white paint [§] to achieve a uniform light emission into the counter volume. The end cap time-of-flight counters are treated in a different way: the fibres are glued, with the help of small plexiglass cylinders, to the end cap light guides. Due to the higher transmission one has to use neutral density filters [§§] which are placed in the coupling pieces between quartz and polystyrene fibres. The

[††] CYANOLITH, 3M, Switzerland; Distributor: Ets. Longo, Geneva.

[†††] Two component glue STYCAST 1264, made by Emerson &Cuming.

[§] Reflector paint PLEX 4171, made by Röhm GmbH, Darmstadt, Germany.

[§§] Kodak wratten gelatine filter No. 96 N.D. 1.00 CAT 149 6405 resp. No. 96 N.D. 0.30 CAT 149 6330.

properties of the fibres are summarized in table 2.

An extra RCA 8575 tube receiving a light pulse from the distribution box serves as a gate generator for shower and time-of-flight ADCs and as a common start for the time-of-flight TDCs.

2.3. Reference detectors

As mentioned above, it is essential to control the laser intensity fluctuations with good precision. For this purpose, we use two independent reference systems:
1) A photodiode (PD) with a high long-term stability §§§ and a low noise two-stage amplifier [4]. The photodiode and preamplifier are placed close to each other in an aluminium pipe to have the signal line as short as possible. The light connection between diode and distribution box is established by a plexiglass rod protected by a steel pipe. The most important properties of the photodiode are summarized in table 3.
2) A lead glass Cherenkov counter (LG) consisting of a 30 cm long block made of SF5 †; its cross section is 14.5×14.5 cm^2. The counter is viewed by an RCA 4525 tube which is glued onto the glass surface. The counter is situated close to the laser and receives its light, similarly to the gate generating tube, via a quartz fibre of 30 m length and a diameter of 0.2 mm from the distribution box. A source of reference light is supplied by the cosmic muons travelling through the block and emitting Cherenkov light along their path.

A cosmic muon is recognized by a four-fold coincidence of scintillation counters, two above and two below the lead glass block. To exclude muons slower than minimum ionizing over the whole length of the lead glass Cherenkov counter, an iron absorber of 10 cm thickness is inserted between the lower two trigger counters. The iron shield also reduces hits from air showers.

Test measurements resulted in a pulse height distribution from cosmic muons with 28% fwhm. To catch the maximum of this distribution, one calculates a "truncated mean". The average rate is 1.8/min. To determine the truncated mean with an accuracy of better than 1%, 150 cosmic events are needed, corresponding to a counting time of roughly 80 min.

2.4. Operation of the monitor system

The monitor system is run once per day. In order to obtain the ratio of laser pulse height per counter to laser pulse height from reference tube with an accuracy of better than 1%, 200 laser pulses per run are needed.

§§§ PD 1900, EMI Gemcom.
† Schott, Mainz.
†† MIK 11/2 with CPU LS1-11 of DEC.

To avoid accidental hits from Bhabha scattering or beam–wall interactions, one has to make sure that there is no beam in the storage ring. Else one gets nonreproducible results especially in the end cap region, due to pick up from the beam through the long ADC gate of 700 ns.

A laser run is controlled by a minicomputer ††. During normal data acquisition, this is used only to accumulate the pulse heights produced by cosmic muons in the lead glass counter. Due to the low rate, cosmic muon pulses are recorded continuously when running the experiment. The shift operator starts a laser run by sending a signal from the online computer PDP 11/45 via a CAMAC mail box to the minicomputer. The minicomputer calculates the ratio $P^i_{\mathrm{TUBE}}/P_{\mathrm{REF}}$ for each shower and time-of-flight counter tube, where, as in eq. (2), P^i_{TUBE} denotes the laser pulse seen by the ith counter and P_{REF} denotes the laser pulse seen by the lead glass reference counter. For the time-of-flight tubes, also TDC values are read. For the data read, the computer accumulates the linear and quadratic sums. In addition, the six lowest bits of each ADC and TDC channel are tested. At the end of the run, after 200 shots are over, the mean, the ratio rms width/mean and a bit control word are computed for each phototube. The bit control word accumulates the information on the six lowest bits: it marks if one of these bits is always or never set. These $3 \times (1984 + 2)$ words are written into the CAMAC mail box together with the current truncated mean and relative rms width for the cosmic muon pulse height distribution. Finally, the mail box is read by the on-line PDP, and the whole monitor event is transferred to the DESY-IBM central computer.

2.5. Time stability of the monitoring system

In fig. 9 the value of MON_i, averaged over all shower counters, has been plotted as a function of monitor runs. This quantity is proportional to the average response of all phototubes to the laser light. A decrease of gain is observed with increasing age of the photomultiplier tubes. This shows the importance of the monitoring procedure; the decrease is corrected for by virtue of eq. (1).

The laser intensity fluctuations are controlled by the reference PM and its cosmic reference light. Fig. 10 shows the truncated mean of the cosmic muon pulse height distribution for all monitor runs performed up to now as a function of time. One recognizes a decrease of pulse height with time that is attributed to a decrease in gain of the reference phototube. At the end of monitor run 146, the high voltage of the reference PM was raised without curing the problem: now the pulse height decreases even faster than before which might be due to the fact that the PM cannot stand the increased high voltage. As a consequence, the lead glass counter was

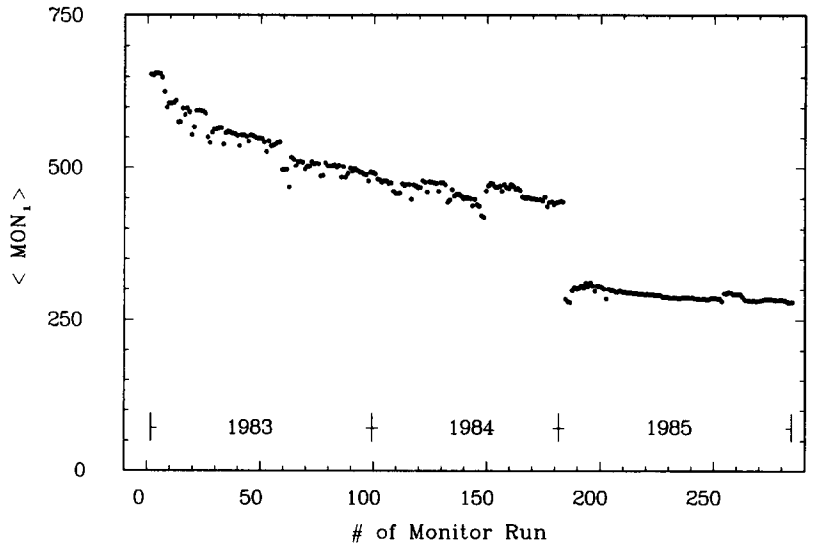

Fig. 9. Time dependence of MON_i, averaged over all shower counters.

Table 3
Properties of the photodiode PD 1900

Cathode type	S-4
Spectral range	300–650 nm
Cathode sensitivity	40 μA/lm
Max. quantum efficiency	12.5%
Dark current	1.5 pA

exchanged after this running period (monitor run 182).

Within wide limits, the gain variations of the reference PM, as seen in fig. 10, do not influence the monitoring precision due to the use of the cosmic reference light in eq. (2). However, if the gain becomes too low, the truncated mean procedure and nonlinearities lead to calibration offsets of a few percent. One handle for finding such effects in the ratio

$$R_{\mathrm{Ref}} = \langle \mathrm{LG} \rangle / \langle \mathrm{PD} \rangle,$$

where $\langle$LG$\rangle$ is the cosmic-corrected response of the reference PM and $\langle$PD$\rangle$ the response of the reference photodiode to the laser light. Fig. 11 shows this ratio as a function of time. About two thirds of the distribution are flat, except for two narrow regions: here, the rapid change of R_{Ref} is explained by the fact that all voltages have been switched off during shut down periods.

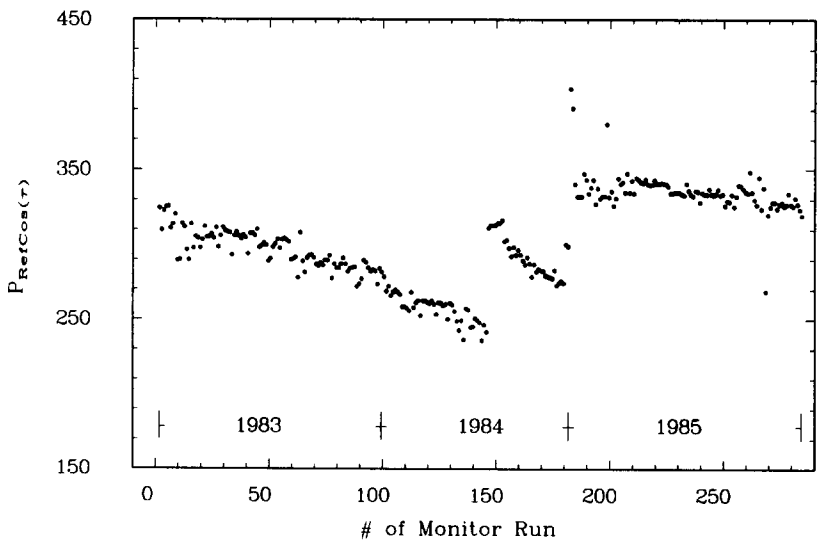

Fig. 10. Time dependence of the truncated mean of the cosmic muon pulse height distribution.

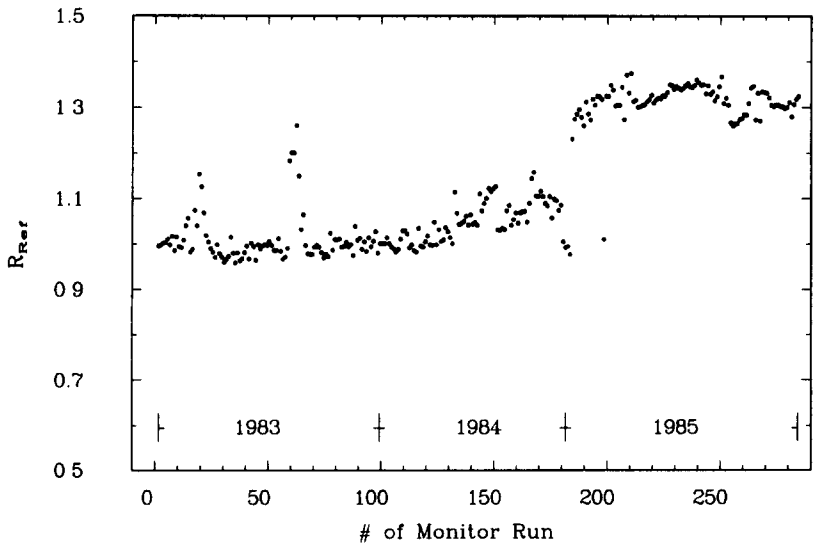

Fig. 11. Time dependence of the ratio lead glass/photodiode.

At monitor run 182, one observes a step which was caused by the exchange of the quartz fibre which transports the laser light from the distribution box to the lead glass counter (fig. 10).

There are, however, aging effects which cannot be corrected for by the monitoring method, as for example radiation damages or any deterioration of scintillator material and optical fibres. These effects can be controlled only by absolutely calibrating the shower counters in definite time intervals, using Bhabha scattering events. Secondly, there are changes to the monitoring system itself which ask as well for an independent method to absolutely calibrate the whole calorimeter. Such a change is for example the exchange of the main quartz fibre because this operation does not cancel from eq. (1). The calibration method and its consequence for maintaining the stability required are discussed in sect. 3.5. The final stability results are presented in sect. 3.6.

3. Calibrating the shower counters

3.1. Introductory remark

To discuss the interplay of monitoring and calibration procedures, we rewrite eq. (1) with the help of the following expressions:

$$E = P_c \epsilon_{cal}, \tag{3}$$

where we derive the energy E from the corrected pulse height P_c and an absolute calibration constant ϵ_{cal}. The determination of the absolute calibration constant is an iterative procedure and will be described in sect. 3.5, after introducing the correction factors to be applied. The corrected pulse height can be calculated from the individual pulse heights of neighbouring shower counters i:

$$P_c = \sum_{i=1}^{n} P^i C_i. \tag{4}$$

Here, P^i denotes the pulse height measured by the ith tube, while n is the number of counters hit by a particle shower, and C_i is a factor to correct for losses and inhomogeneities in the shower detector. Four major sources of losses contribute to the correction factor C_i so that it breaks up into a product as follows:

$$C_i = C_1 C_2(E, \theta) C_3(\phi) C_4^i(\tau). \tag{5}$$

Note that the first three factors do not depend on time, while the last one accounts for time variations of the pulse height measurement. In eq. (5) C_1 refers to the ratio of energy deposited to energy detected and is discussed in sect. 3.2. C_2 corrects for polar angle dependent leakages and losses of shower particles, and for variations of the light collection with impact point of the detected particle. It is discussed in detail in sect. 3.3. The losses of shower energy depending on the azimuthal angle are summarized by C_3. For charged particles, this correction depends in a complicated way on their momenta and charges, the strength of the magnetic field, and the azimuth. Therefore they are considerd only for photons. Details are discussed in sect. 3.4.

C_4, finally, takes into account gain variations of the photomulipliers. This factor is time dependent since the gain of the phototubes shows a long term variation. Moreover, changes of the high voltages applied to the different multiplier tubes turned out to be necessary from time to time, imposing a change of C_4. The entire

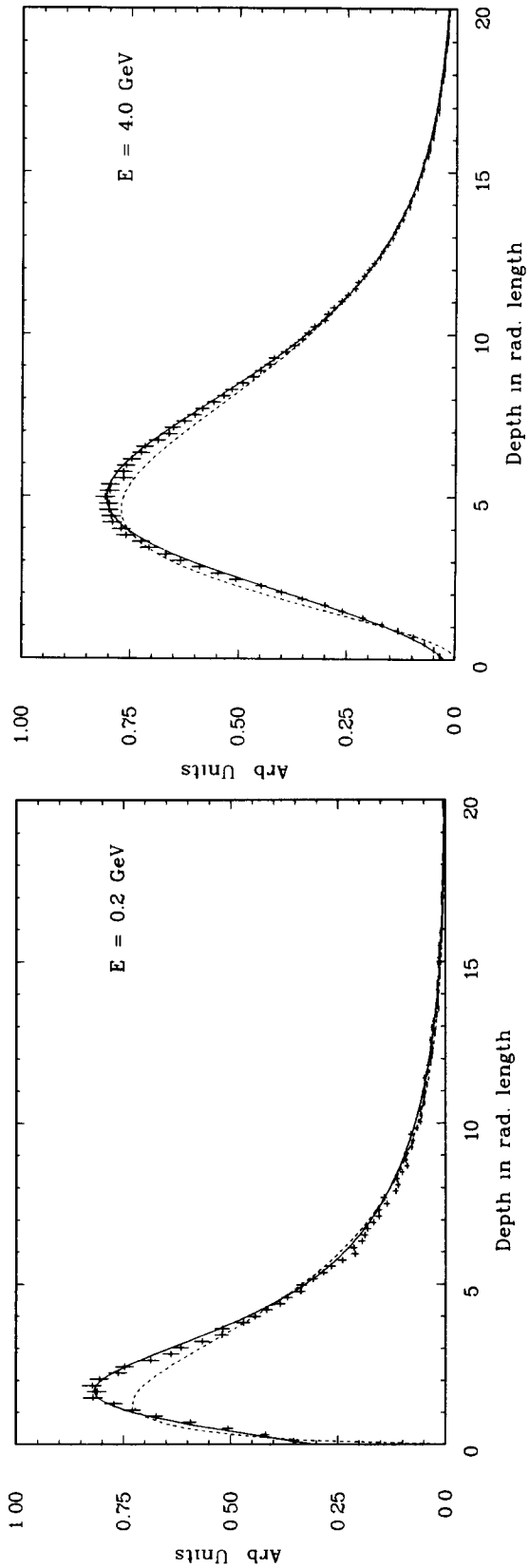

Fig. 12. A shower profile: energy deposited as a function of depth, for an EGS simulated shower at 0.2 GeV. dashed: parametrization accoriding to eq. (7). full: parametrization according to eq. (8) (left). Same as fig. 12a, for a 4 GeV shower (right).

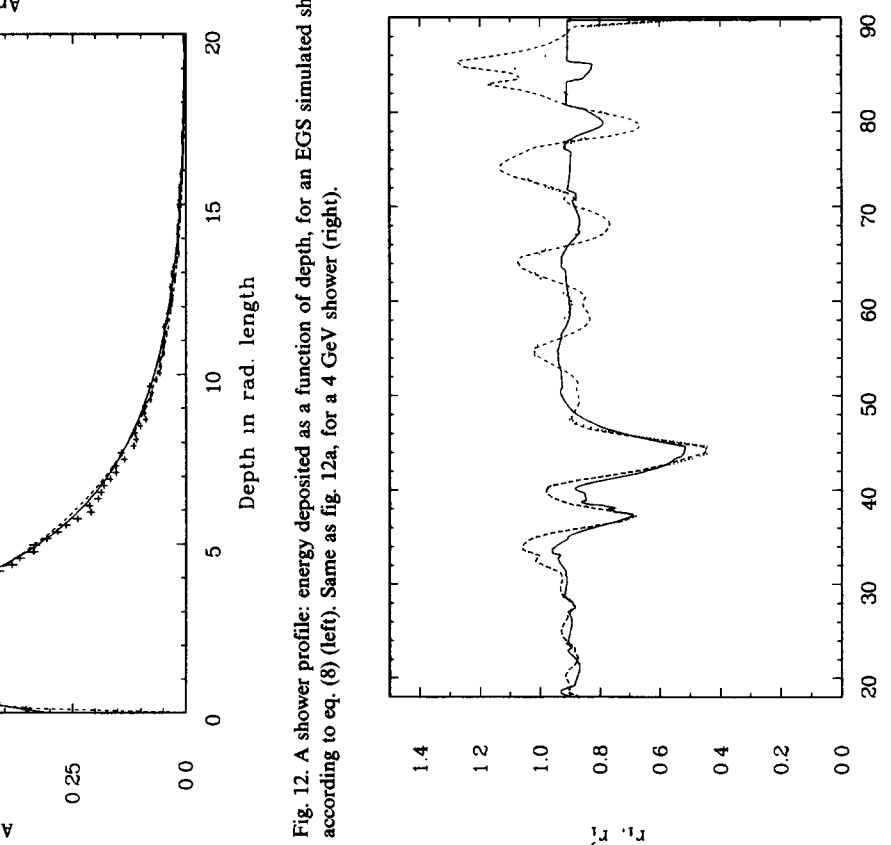

Fig. 13. Ratio of deposited energy/beam energy as a function of the polar angle ($E = 5$ GeV); full line: ratio r_1 dotted line: ratio r_1', including eq. (9) for plane parallel counters dashed line: ratio r_1' including eq. (9) for wedge counters.

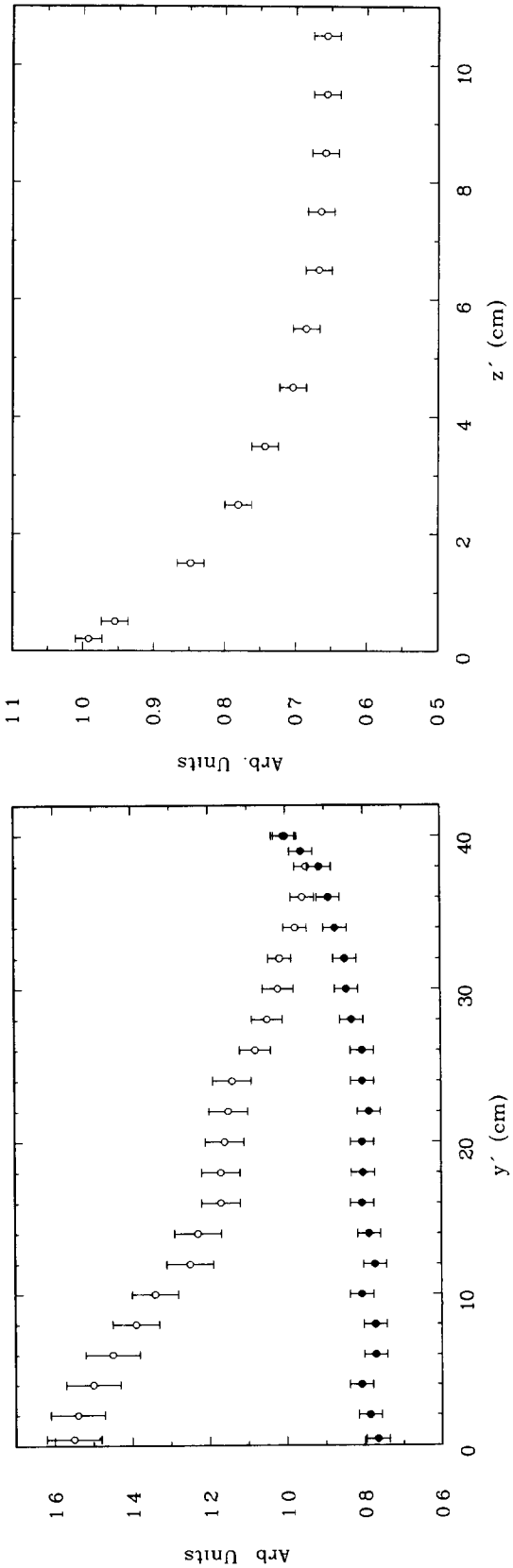

Fig. 14. Pulse height as a function of the depth y'; open points: wedge module; full points: plane parallel module (left). Pulse height as a function of the distance z' from the wave length shifter (right).

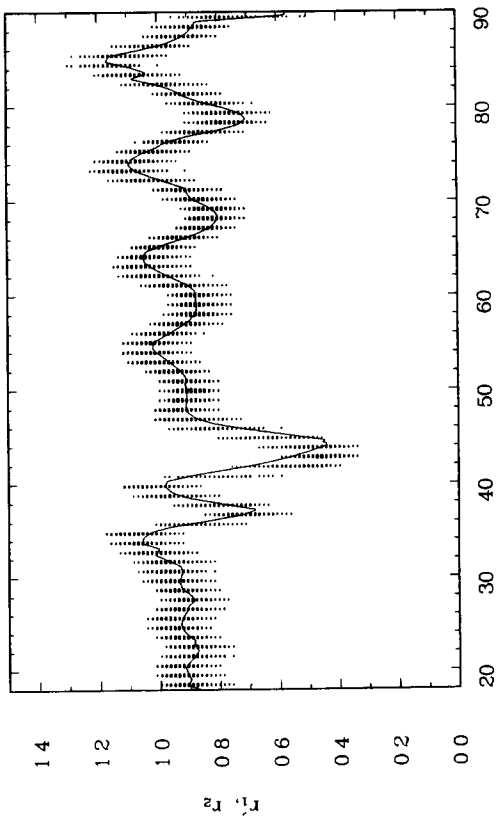

Fig. 15. Ratio of deposited energy/beam energy from Bhabha scattering electrons; measurement (r_2) and Monte Carlo result (r_1).

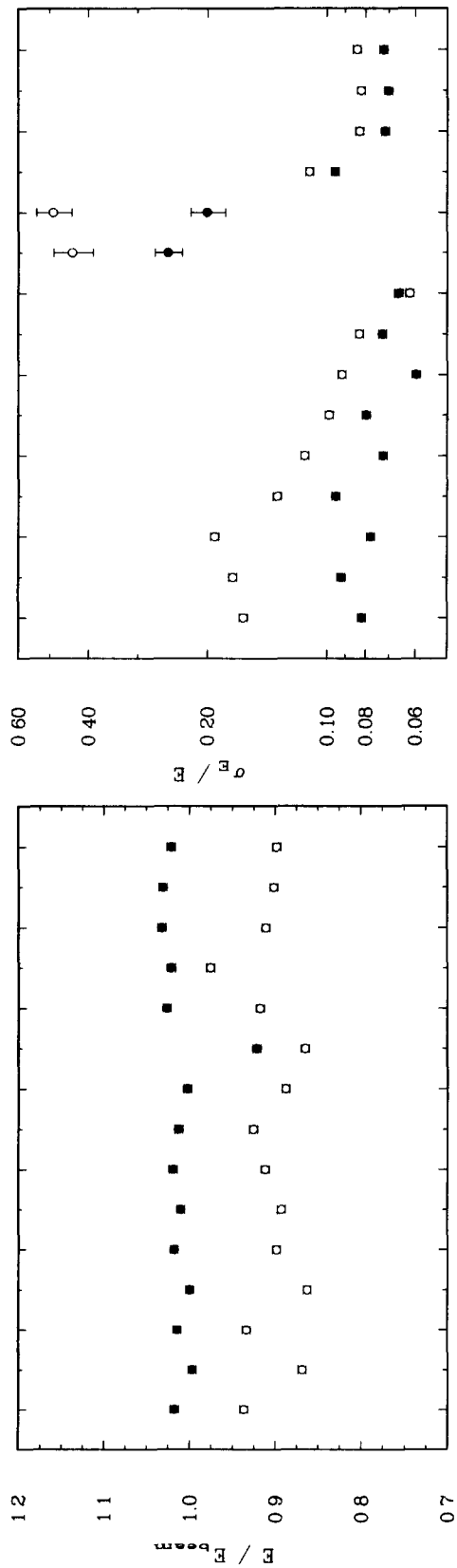

Fig. 16. Ratio of deposited energy/beam energy from Bhabha scattering electrons as a function of shower counter ring number (ring 1 = 90°, ring 15 = 20° in polar angle); full points: corrected energy; open points: without correction factor C_2 (left). Relative energy resolution (right).

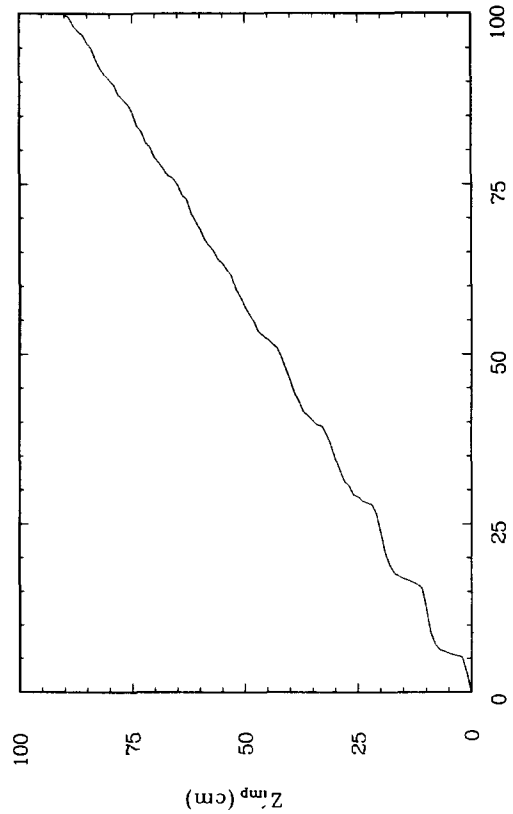

Fig. 17. Relation between real impact point and calculated centre of gravity for 0.5 GeV photons.

machinery of monitoring devices described in sect. 2 is therefore focused onto this special parameter which can therefore be identified with the third factor in eq. (1).

3.2. Corrections for energy escaping detection

The factor

$$C_1^{-1} = \frac{E_{\text{vis}}}{E_{\text{dep}}}, \tag{6}$$

equals the amount of energy E_{vis} detected in the scintillator as compared to the energy E_{dep} deposited in the whole shower counter. This constant which depends on the relative density of scintillation and inactive material (mainly lead) was determined by Monte Carlo calculations using the EGS code [5a] and amounts to $C_1 = 2.77(3.77)$ for the barrel (end cap) counters [5b].

3.3. Corrections for losses depending on the polar angle

Particles hitting different modules of the ARGUS shower detector will produce light, the amount of which depends on the polar angle of the impact direction: inactive material (support structure of the shower counters, holes between modules) reduces the amount of energy detected by the scintillator. Moreover, the relative amount of light produced in the scintillator and transported to the photomultiplier depends on the position where it was produced. Additional losses occur inside the counter module, e.g. when transporting the light through wavelength shifter and light guide to the photomultiplier.

The photon detection system measures the energies of electrons and positrons, too. Since for charged particles the drift chamber information is available, polar and azimuthal angles are known already when starting the shower counter analysis. For photons, however, determination of these quantities is part of the shower reconstruction itself.

In order to determine the influence of losses depending on the particle impact direction, one has to simulate the shower counter system in a Monte Carlo procedure: one must trace the electromagnetic shower through the detector and simulate the deposit of the appropriate amounts of energy in the different materials traversed. Only the longitudinal development of the shower was taken into account: changing the parameters controlling the transverse extension turned out to be of negligible influence. This approximation simplified the problem considerably and allows one to use an analytic expression for the longitudinal shower shape to save computer time. We have parametrized the longitudinal shape by the expression proposed by Longo et al. [6]:

$$\frac{\mathrm{d}E}{\mathrm{d}t} = At^{\alpha}\,\mathrm{e}^{-\beta t}, \tag{7}$$

where t measures the longitudinal shower extension in units of the radiation length, and A, α, and β are constants.

The above equation can be expressed in a more convenient form when one introduces the differential energy $(\mathrm{d}E/\mathrm{d}t)_{\max}$ in the shower maximum, and $t_{\max}$, the longitudinal position of the shower maximum:

$$\frac{\mathrm{d}E}{\mathrm{d}t} = \left(\frac{\mathrm{d}E}{\mathrm{d}t}\right)_{\max}\left(\frac{t}{t_{\max}}\right)^{\alpha}\mathrm{e}^{\alpha(1-t/t_{\max})}. \tag{8}$$

This expression describes only approximately the Monte Carlo generated shower distribution (fig. 12, dashed curve). Unfortunately, the corrections to be applied turned out to be sensitive to the deviations from eq. (8). Hence we had to improve eq. (8) by introducing a t-dependence of α [7]. As demonstrated by figs. 12 a and b, for electrons of 0.2 GeV and 4.0 GeV respectively, one achieves an excellent agreement between the fit and the Monte Carlo distribution with the improved parametrization over a broad energy range (full curve).

The correction factor C_2 was determined in two steps in order to study the influence of the different sources responsible for losses in detected energy. Tracing the shower through the detector and considering the support structure, holes in the detector, the wave length shifter, and the leakage due to the finite length of the counters, the ratio

$$r_1 = \frac{E_{\text{dep}}}{E_{\text{p}}},$$

was determined. E_{dep} is the amount of energy deposited in the active (scintillator) and passive (lead) components of the shower counter modules, while E_{p} is the energy of the traced electron. The parameter r_1 as a function of the polar angle of the point of the particle's incidence on the shower counter is plotted in fig. 13 for 5 GeV electrons (full line). The wiggles observed in fig. 13 can be explained by well known inhomogeneities of the shower detector, as for example support structure, wave length shifter, and holes in the detector.

A further polar angle dependence of the light output from the shower counter is due to the variation of light transport from various parts of a counter module to the photomultiplier. In order not to rely on Monte Carlo simulations of the light transport process, which depends sensitively on the reflection coefficients of the different surfaces involved, we have collected the necessary information in a test beam [8]. We scanned the test counter with a collimated electron beam incident in a plane orthogonal to its longitudinal axis, the beam coming parallel to the scintillator plates, i.e. parallel to the x'-axis, see fig. 2c. Measurements were performed at different longitudinal depths (y'), and varying distances (z' coordinate) between the wavelength shifter and the beam impact point. The results of this measurement are plotted in fig. 14 a,b. They have been parametrized by a

function factoring as

$$W(z', y') = f(z')g(y'), \tag{9}$$

$$\int W(z', y')\, dz'\, dy' = 1. \tag{10}$$

Folding this expression for the light collection in different parts of a shower module with the deposited energy, one arrives at an improved description of the ratio r_1'. The ratio r_1' is included in fig. 13 for a plane parallel (dotted curve) and a wedge counter (dashed curve). The quality of these calculations can be checked by comparing the value r_1' (fig. 15, full line) with the relative amount of energy deposited by a 5 GeV electron from Bhabha scattering in the shower counters:

$$r_2 = \frac{E_{\text{dep}}}{E_{\text{p}}} = \sum_{i=1}^{n} p^i C_1 C_4^i(\tau) \frac{\epsilon_{\text{cal}}^i}{E_{\text{p}}}. \tag{11}$$

The data and the Monte Carlo predictions are in good agreement. Note that the polar angle interval in which the shower energy of an electron is deposited is much broader than the structures observed in fig. 15. Hence the observed agreement between the results of the Monte Carlo calculations and the data is a real check of the procedure to determine the correction factor

$$C_2(E, \theta) = \frac{1}{r_1'(E, \theta)}. \tag{12}$$

The correction factor was determined at five energies by a Monte Carlo calculation. Parametrizing the energy dependence with the help of a polynominal, $C_2(E, \theta)$ can be calculated for other energies.

Applying the combined correction factor

$$C_i = C_1 C_2(E, \theta) C_4^i(\tau). \tag{13}$$

to the measured pulse height of an electron from Bhabha scattering, one arrives at the results for the ratio E/E_{beam} and the resolution $\sigma(E)/E$ plotted in fig. 16 a, b (full points), as a function of the ring number: ring $1 \simeq 90°$, ring $10 \simeq 45°$, ring $15 \simeq 20°$, see fig. 1. For comparison the results before applying the correction factor $C_2(E, \theta)$ are also shown (open points). The dramatic improvement of the energy resolution in the region of the detector where the barrel and end cap counters merge (rings 9–12) demonstrates best the progress achieved.

The resolution can be parametrized by the expression:

$$\frac{\sigma(E)}{E} = \sqrt{0.072^2 + \frac{0.065^2}{E(\text{GeV})}},$$

in the barrel, averaged over rings 1 to 9, and

$$\frac{\sigma(E)}{E} = \sqrt{0.075^2 + \frac{0.076^2}{E(\text{GeV})}}, \tag{14}$$

in the end cap region. The constant term is mainly due to contributions from the support structure.

3.4. Energy corrections for photons

The energy correction factor depends on the polar angle as discussed above. In addition, an azimuthal angular dependent correction of the energy has to be considered for photons because the shower counter modules point directly to the beam line; hence an appreciable amount of energy can be lost in the support structure. To apply the θ and ϕ dependent correction factors $C_2(E, \theta)$ and $C_3(\phi)$, one has first to determine the azimuthal and polar angle of the photon impact point on the shower counter. Therefore the coordinates of the photon impact point and its energy must be determined in an iterative procedure.

3.4.1. Reconstructing the coordinates θ and ϕ of the photon impact point

The algorithm to derive the photon impact coordinates was developed and checked in a Monte Carlo simulation. Photons of 0.5 GeV and 5 GeV have been generated at the vertex and tracked through the full detector. The polar angle of the photon was derived from the centre of gravity

$$u(s) = \frac{\sum_{i=1}^{n} u_i p_i}{\sum_{i=1}^{n} p_i}, \tag{15}$$

n is the number of counters hit by a photon shower, p_i the corresponding pulse height recorded and u_i the value of the coordinate of the centre of the shower counter module i. For the barrel shower counters the z-axis, parallel to the direction of the solenoid axis ($u_i = z_i$) was used, while for an end cap counter its radial distance r_i from the solenoid axis was chosen ($u_i = r_i$). The correlation between the real impact point z_{imp} and the calculated centre of gravity z_s for photons of 0.5 GeV hitting the barrel counters is plotted in fig. 17. The function z_s for two energies (0.5 and 5 GeV) is available in tabulated form for the analysis. The corresponding relation for other energies was determined by interpolation (extrapolation), assuming a logarithmic dependence on the photon energy.

Energy E and polar angle θ of the photon have been determined in an iterative procedure in order to take into account the energy dependence of the correction factor $C_2(E, \theta)$. The iteration converged quickly. The quality of the θ reconstruction can be judged from fig. 18 which shows the reconstructed polar angle in comparison with the polar angle of the impact point as given by the Monte Carlo input (for 5.0 GeV photons). The bad reconstruction at $\theta = 45°$ is due to the large

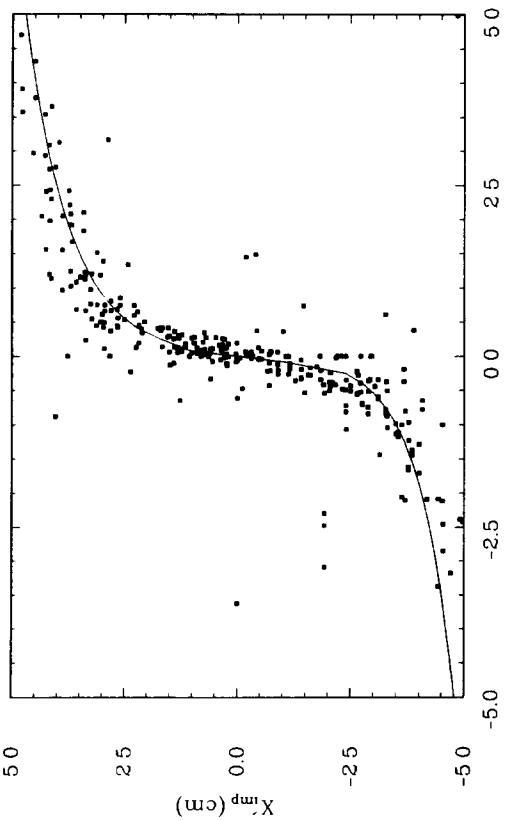

Fig. 19. Relation between real impact point x'_{imp} and calculated centre of gravity x'_s.

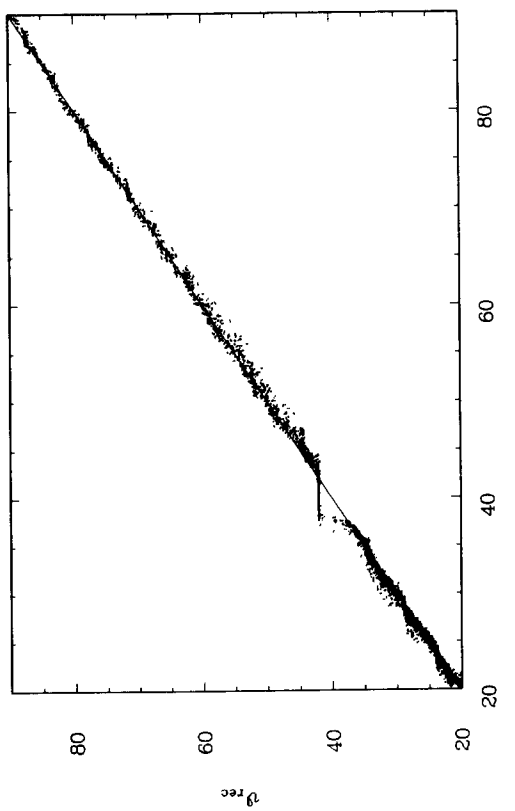

Fig. 18. Comparison of polar angle as given by Monte Carlo, and reconstructed angle.

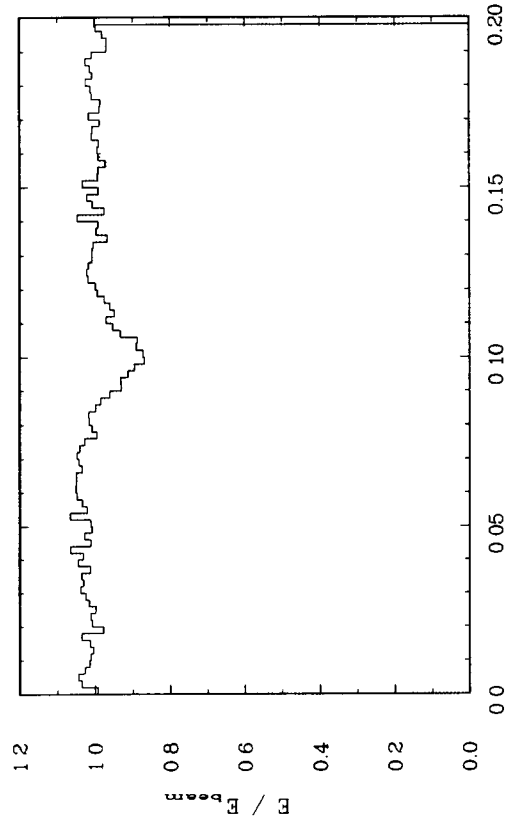

Fig. 20. Corrected (full line) and uncorrected (dotted line) ratio energy deposited/beam energy as a function of azimuthal angle.

size of the corresponding shower counter.

The azimuthal angle of the photon impact point is derived from the cartesian coordinate

$$x'_s = \frac{\sum x'_i p_i}{\sum p_i}, \tag{16}$$

where the coordinate x'_i is measured in the front plane of a shower counter module perpendicular to the z direction, see fig. 2c. $x'_i = 0$ is defined as the centre of the counter module i with the maximal pulse height. The correspondence between x_s and the real photon impact point x_{imp} was derived from Monte Carlo data (fig. 19). They have been parametrized for general use in the analysis program. The function x'_s turned out to be energy independent to good approximation.

3.4.2. Energy corrections depending on the azimuthal angle

Since the support structure of the shower counters points towards the beam line, appreciable energy losses are expected for narrow azimuthal angular intervals. This is demonstrated by fig. 20, where the reconstructed energy E of photons from the process $e^+e^- \to \gamma\gamma$, normalized to the beam energy, is plotted as a function of the azimuthal angle of the reconstructed impact point (dotted line):

$$E = P_c \epsilon_{cal} C_1 C_2(E, \theta) C_4(\tau). \tag{17}$$

The holes at $\phi = 0$ and 0.2 rad are due to losses in the support structure. Monte Carlo simulations show that their shape and depth are energy independent. The hole at $\phi = 0.1$ rad is due to losses in the region between counter modules, and gets washed out at lower energies. Therefore we have corrected only the losses in the support structure. The dependence of the ratio E/E_{beam} after applying the correction factor $C_3(\phi)$ has also been entered in fig. 20 (full line). It demonstrates the homogeneity achieved. The improvement in energy resolution is demonstrated by fig. 21, where the measured photon spectrum from $e^+e^- \to \gamma\gamma$ is plotted before and after applying the correction factor $C_3(\phi)$.

3.5. Determination of the absolute calibration constant ϵ_{cal}

The correction factors C_1, C_2, C_3 described in the preceding sections correct for energy losses in the calorimeter. The last term in eq. (3) is the absolute calibration constant ϵ_{cal} which converts measured and corrected pulse heights into energies. This absolute calibration can be performed using electrons and positrons from Bhabha scattering processes. The Bhabha cross section is high enough to allow for a calibration of all shower counters based on a data sample of about 7 pb^{-1}, corresponding to approximately 5×10^5 Bhabha events.

The impact points of the electron tracks on the shower counters are derived from the drift chamber track reconstruction. The electron energies E_p are known very accurately from the machine energy if the Bhabha tracks are selected in such a way that energy losses due to radiation are minimized.

After selecting an electron or positron track, the ratio of shower energy measured and the energy which should be deposited for this track (eq. (12)), can be calculated for each Bhabha event k:

$$r_3^k = \frac{\sum_{j=1}^{n} P^j C_1 C_4^j(\tau) \epsilon_{cal}^j / E_p}{r_1'(E_p, \theta)}, \tag{18}$$

r_3^k is a correction factor for the whole cluster, i.e. for the group of shower counters which have been hit by the electromagnetic shower. From this the absolute calibration constant for each counter can be computed in the following way:

$$w_k^i = \frac{P^i C_1 C_4^i(\tau) \epsilon_{cal}^i}{\sum_{j=1}^{n} P^j C_1 C_4^j(\tau) \epsilon_{cal}^j}, \tag{19}$$

$$\frac{1}{\epsilon_{cal}^i} = \frac{\sum_k r_3^k w_k^i}{\sum_k w_k^i}, \tag{20}$$

ϵ_{cal}^i is the average over all clusters to which the counter i has contributed.

The whole procedure is now repeated up to twenty times for a given sample of Bhabha events. For the first step, ϵ_{cal}^i is set to 1, whereas for the following iterations the preceding value of ϵ_{cal}^i is used.

3.6. Stability of the calibration

The factor $C_4^i(\tau)$ in eq. (5), correcting for the varying gain of the photomultipliers is time dependent and needs monitoring. For this purpose we have used the laser system described in sect. 2. As shown in sect. 2.1., the gain correction factor $C_4^i(\tau)$ at a time τ can be derived from the one determined at a fixed $\tau = 0$ for each shower counter module by:

$$C_4^i(\tau) = \frac{\mathrm{MON}_i(0)}{\mathrm{MON}_i(\tau)}. \tag{21}$$

As mentioned in sect. 2.5, the monitoring is checked by recalibrating with Bhabha events in certain time intervals. This has been done by dividing the total running time of up to now three years into 19 intervals. For each period a separate calibration of all counters was performed, as described in sect. 3.5. Gain variations during these periods were followed with the laser monitor system.

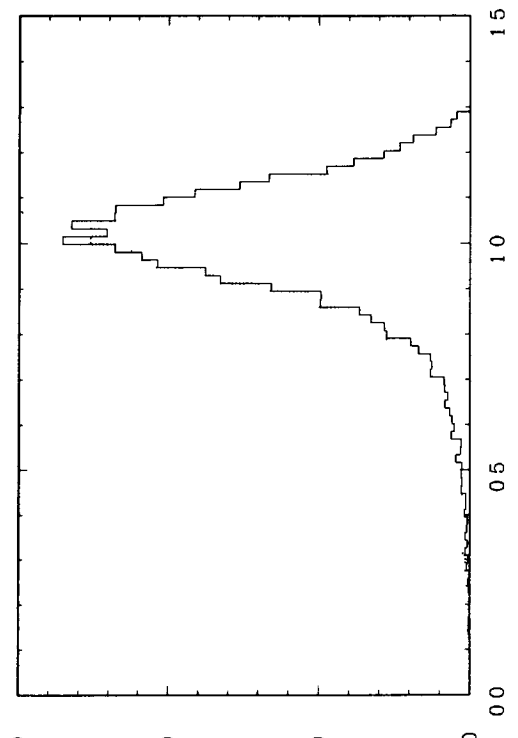

Fig. 21. Corrected (full line) and uncorrected (dotted line) photon energy spectrum of the process $e^+e^- \to \gamma\gamma$.

Fig. 22. Ratio energy deposited/energy reconstructed for barrel counters, as a function of time (left). Ratio energy deposited/energy reconstructed for end cap counters, as a function of time (right).

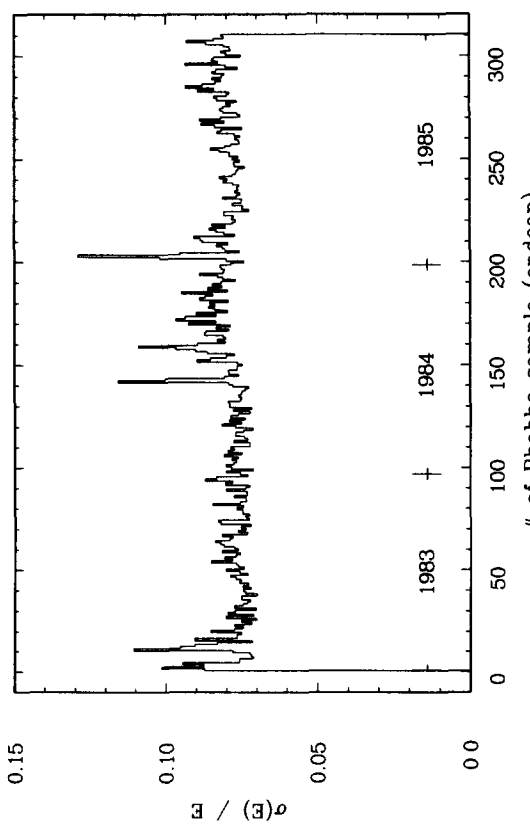

Fig. 23. Energy resolution σ_E/E for Bhabha electrons.

Fig. 24a. Reconstructed π^0-mass as a function of time.

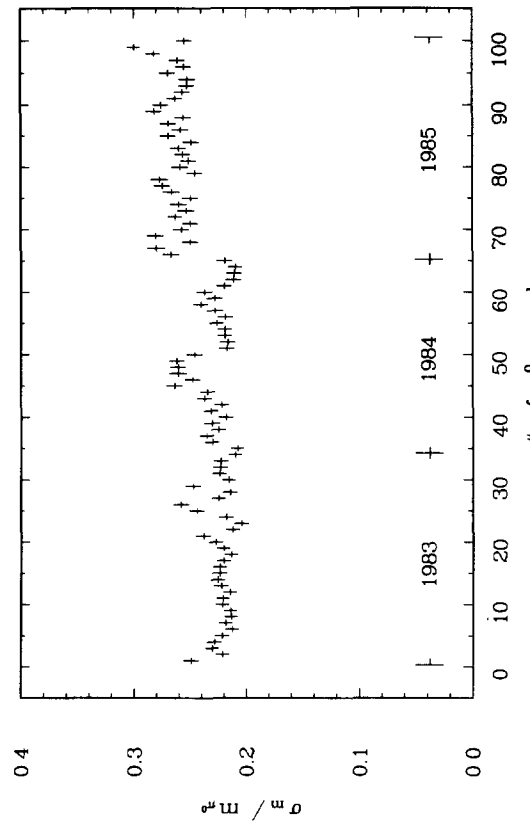

Fig. 24b. Relative width $\sigma(m_\pi)/m_{\pi^0}$ of the π^0 signal as a function of time.

The ratio E/E_{beam} for electrons from Bhabha scattering, averaged over all counters, has been determined as a function of time (fig. 22 a,b). No variation of this ratio for the barrel counters (fig. 22 a) and end cap counters (fig. 22b) is observed. Any deterioration of the shower counter system over long time periods due to radiation or aging effects would be corrected for by applying these 19 calibration constants. As a matter of fact, no such deterioration is observed in the ratio E/E_{beam} for the 1985 data without recalibration.

In view of the large radiation damage observed in other experiments [9] it is interesting to note that the counters have been operated in an inert nitrogen atmosphere from the very beginning. The main effect of the recalibration procedure is an improvement of the energy resolution. The resolution achieved after all corrections is shown in fig. 23. For the 1985 data, the resolution improves from 8.0% to 7.5% after recalibrating with Bhabha events.

To check all the algorithms used to determine the energy of electromagnetic showers at low energies, we have reconstructed π^0's using photons with $E_\gamma > 50$ MeV. The data sample used for this analysis corresponds to a total luminosity of 151.5 pb^{-1}. These data have been divided into subsamples to study the variation of the π^0-mass with time. For each of these subsamples the invariant mass of all two-photon combinations has been calculated. The background has been determined by event mixing, and subtracted after normalization. The resulting spectrum shows a clear π^0-peak to which a Gaussian has been fit. In fig. 24 the π^0-mass as well as the relative width of the peak has been plotted for the different data samples. Both photons have been detected in the barrel shower counters. The fitted π^0-mass decreases by 4 MeV over a period of three years. By reconstructing π^0s with one photon detected in the shower counters, and the second one measured as a converted photon in the drift chamber, we make sure that the observed effect is not generated by the method applied to determine and subtract the background under the π^0-signal.

This observation may be explained by the influence of the ADC threshold affecting each single shower counter: the steady decrease of the photomultiplier gain results in a effectively rising ADC threshold. In contrast to electrons of 5 GeV/c momentum, the energy determination for low energy photons is very sensitive to this effect.

4. Using the monitor system for the time-of-flight counters

The laser system monitors also the time-of-flight counters. Here the pulse heights are not converted into physical quantities but used for time walk corrections in the off line calibration. Their absolute values are of no direct interest and need not be controlled. The monitoring system serves to check whether tubes and readout electronics are working properly, and is used for calibrating the time-of-flight TDCs.

Calibrating the TDCs is done plugging a switch delay unit in the TDC common start circuit and performing laser runs for well defined delay steps. The switch delay has previously been absolutely calibrated to an accuracy of ± 25 ps [1b].

5. Summary

Monitoring with a central laser light source in combination with an absolute calibration using leptons from Bhabha scattering processes turned out to provide a sufficient means to correct for all time dependent variations of the ARGUS shower calorimeter. The laser monitor system is efficient to correct for medium term time variations of the detector response, while long term variations are controlled with the help of Bhabha scattering events. The energy collected in the calorimeter has to be corrected for losses due to longitudinal leakage, absorption in the support structure, and reduced showering in the wavelength shifter read out system. It is demonstrated that these corrections can be determined with high precision so that finally the energy resolution of the calorimeter is limited at high energies by fluctuations of the losses in the support structure, and at low energies by sampling fluctuations.

Acknowledgements

We gratefully acknowledge the help from our colleagues of the ARGUS collaboration whose cooperation made this analysis possible. We thank Prof. W. Hofmann and Dr. A. Markees for their help during the construction phase of the shower counter system. We thank the workshops of the institutes at DESY, Dortmund, and Heidelberg for their technical support, especially K. Schmidt and the late Dr. M. Vysočanski of the Electronic Workshop at the Heidelberg institute. We would like to thank Dr. W. Trost, Physikalisches Institut der Universität Heidelberg, for assistance in using the Heidelberg betatron for irradiation studies. We appreciate the excellent cooperation with J. Laaber Faseroptik GmbH, Rüsselsheim. We thank the DESY directorate for the support and the kind hospitality extended to us. This work was supported by the Bundesministerium für Forschung und Technologie of the Federal Republic of Germany.

References

[1] a M. Danilov et al., Nucl. Instr. and Meth. 217 (1983) 153.
b R. Heller et al., Nucl. Instr. and Meth. 235 (1985) 26.
c A. Drescher et al., Nucl. Instr. and Meth. 205 (1983) 125.
A. Drescher et al., Nucl. Instr. and Meth. 216 (1983) 35.
d A. Arefiev et al., DESY 83-025 (unpublished).

[2] R. Heller, Diplomarbeit, Heidelberg 1979 (unpublished).

[3] B. Powell et al., Nucl. Instr. and Meth. 198 (1982) 217.

[4] R. Heller, Thesis, IHEP-HD/84-08, Heidelberg 1984 (unpublished).

[5] a R.L. Ford and W.R. Nelson, SLAC-210, UC-32 (1978).
b A. Drescher, Diplomarbeit, Universität Dortmund, 1982 (unpublished)/H. Scheck, Diplomarbeit, Universität Dortmund, 1983 (unpublished).

[6] E. Longo and I. Sestili, Nucl. Instr. and Meth. 128 (1975) 283.

[7] U. Matthiesen, Thesis, University of Dortmund 1986 (in preparation).

[8] B. Spaan, Diplomarbeit, University of Dortmund 1985 (unpublished).

[9] Y. Sirois and R. Wigmans, Nucl. Instr. and Meth. A240 (1985) 262.